Research Article

Journal of Environmental Nanotechnology

Synergetic Effect on Electrochemical Performance of Activated Carbon - Multiwalled Carbon Nanotubes Supercapacitor using various Electrodes in Aqueous Electrolyte

D. Thillaikkarasi[1*], R. Ramesh[2]

[1]PG & Research Department of Chemistry, Chikkanna Government Arts College, Tiruppur, TN, India
[2]Department of Physics, Energy and Functional Materials Laboratory, Periyar University, Salem, TN, India
Received: 13.05.2022 Accepted: 19.05.2022 Published: 30-06-2022
*thillaikkarasidhanapal@gmail.com

ABSTRACT

An Electrical double-layer capacitor (EDLC) has been fabricated with activated carbon (AC) and multi-walled carbon nanotubes (MWCNTs), which in turn were synthesized from *Pongamia pinnata* fruit shell and its seed oil, respectively. The activated carbon was produced by the chemical activation process at varying carbonization temperatures from 600-900 °C for 5 hours in N_2 atmosphere. The obtained activated carbon had a high surface area of 1170 $m^2 g^{-1}$ and a total pore volume of 0.5907 $cm^3 g^{-1}$. The surface area of MWCNTs was 216.1 2 $m^2 g^{-1}$ and the total pore volume was 1.5067 $cm^3 g^{-1}$. The as-prepared AC and MWCNTs were characterized by surface area analysis using Brunner-Emmett-Teller method (BET), X-ray diffraction analysis (XRD), X-ray photoelectron spectroscopy (XPS), Raman spectroscopic analysis, Field emission scanning electron microscopy (FESEM), High-resolution transmission electron microscopy (HR-TEM), Energy-dispersive X-ray spectroscopy (EDAX) and DFT (Density functional theory). The electrochemical performance of AC-MWCNTs (25:75) Stainless steel (SS) electrode and Graphite sheet electrode (GE) were studied by cyclic voltammetry, Galvanostatic charge-discharge and electrochemical impedance spectroscopy using 0.5 M Na_2SO_4 aqueous electrolyte. It has shown a specific capacitance of 174 Fg^{-1} and 95.26 Fg^{-1} respectively, using the three-electrode system at a current density of 1 mA g^{-1}. The AC-MWCNT (25:75) SS electrode has exhibited excellent specific capacitance (C_{SP}) and its Specific energy density and Power density were greater than AC-MWCNT (25:75) GE. The electrochemical performance of AC-MWCNT (25:75) SS electrode was identified as a suitable, low-cost and promising energy storage device for future generations. The present investigation attempts to promote the supercapacitor device in the context of available and future technologies for alternative energy systems with outstanding performance.

Keywords: Biomass; Activated carbon; Carbon nanotubes.

1. INTRODUCTION

Electrochemical capacitors (ECs) are studied extensively as energy storage systems for a variety of applications. The emerging choice of supercapacitors is due to their higher power density and longer life cycle in wearable devices, gadgets, communication devices, hybrid electric vehicles, etc. (Simon *et al.* 2014; Li *et al.* 2016). Supercapacitors have renewed potential for market penetration and have become the dominant technology in energy harvesting systems, power grids and large wind turbine pitch control applications (Qu *et al.*2011). Supercapacitors are also known as electrochemical capacitors or ultracapacitors. Depending upon the energy storage mechanism, they can be classified as pseudo-capacitors, hybrid capacitors and electrical double-layer capacitors (EDLCs).

In an EDLC, the capacitance originates due to the build-up of electrical charges in the boundary between the electrode and electrolyte. Hence, the energy storage of capacitors can be tuned by regulating the surface area and pore size of the electrodes and the conductivity of the electrolyte (Aval *et al.* 2018; Shi *et al.* 2011). Supercapacitors have several advantages over conventional storage systems, including lithium-ion batteries. Supercapacitors exhibit enhanced power density, improved cyclic stability and high efficiency. Moreover, they require only a concise time for charging (Miller and Simon, 2008; Brownson, *et al.* 2011; Augustyn *et al.* 2014; Simon and Gogotsi, 2008). In addition, since they can be transported effortlessly, they are preferred as energy sources for electric and hybrid vehicles (Liu *et al.* 2010). Therefore, the development of low-cost electrode materials for EDLCs using carbon-based materials, carbon nanotubes (Ibukun *et al.* 2018; Karthikeyan, 2012; Mageswari *et al.* 2017; Karthikeyan, 2013) and graphene and mesoporous carbon electrodes has gained momentum. The activated carbon-based electrode materials are the right choice for large-scale production of high-performance supercapacitors due to their high specific capacitance, energy density, eco-

friendly nature and low cost (Karthikeyan *et al.* 2008; Sivakumar *et al.* 2012).

Activated carbon-based supercapacitors can be derived from cheap biomass such as *Moringa oleifera* fruit shell, groundnut shell, coconut shell, rotten carrot, etc. (Palisoc *et al.* 2020; Muthu Balasubramanian *et al.* 2020; Jain and Tripathi, 2014; Ahmed *et al.* 2018; Zhou *et al.* 2018; Mandal *et al.* 2021; Niu *et al.* 1997). The porous activated carbon-based electrode derived from rotten carrot (Ahmed *et al.* 2018) showed a specific capacitance of 135.5 Fg^{-1} at 10 MHz in aqueous electrolyte and the highest specific energy of 29.1 Wh kg^{-1} at 2.2 Ag^{-1}. Carbon nanotube-based symmetric supercapacitors (Zhou *et al.* 2018) exhibit the highest specific energy of 72.2 Wh kg^{-1} at a power density of 686.0 W kg^{-1}. The high performance of CNT/graphene nanofiber (GNF) hybrid supercapacitors is attributed due to the sufficient accessible sites for charge storage and the capability of CNT skeleton channels to promote charge transport (Palisoc *et al.* 2020). An AC-MWCNTs symmetric supercapacitor has been reported to deliver a specific capacitance of 122 F g^{-1} at a current density of 0.5 A g^{-1} with a maximum specific energy of 17 Wh kg^{-1}. The metal oxide was incorporated to improve the cyclic stability and storage capacity to make it a hybrid composite electrode (Mandal *et al.* 2021). The AC/MWCNT-$ZnFe_2O_4$ supercapacitor showed a specific capacitance of 609 Fg^{-1} at a current density of 1 A g^{-1}. Another CNTsheet electrode showed maximum specific capacitance of 102 Fg^{-1} at 1 Hz using 38 wt. % as the electrolyte (Niu *et al.* 1997).Incorporating CNTs in AC can be a new technique for creating suitable conducting paths with better porosity that may enhance the performance of supercapacitors. Multiwalled-carbon nanotubes have high electrical conductivity and excellent chemical stability (Yoon *et al.* 2004). According to literature reports, EDLC fabricated from multi-walled CNT showed high specific capacitance in the range 4–135 Fg^{-1} (Emmenegger *et al.* 2003; Signorelli *et al.* 2009; Hu *et al.* 2009).

This current research presents the electrochemical performance of AC-MWCNTs (25:75) symmetric supercapacitors. The active materials can be prepared from cost-effective and environment-friendly natural biomass. The electrochemical performance of AC-MWCNTs (25:75) electrode was studied using three-electrode configuration in 0.5 M Na_2SO_4 aqueous electrolyte. The essence of this work based on the preparation ratio of active materials. Thus, activated carbon weight percentage is standard, and the concentration is varied by adding a percentage from (25% up to 75%) (Show, 2008). Fabrication of ideal polarizable electrode with activated carbon and MWCNTs with super carbon black (SP) as (25:75) %, (50:50) % and (75:25) %. Based on the electrochemical performance, AC-MWCNTs (25:75) symmetric supercapacitor electrode showed best output results in 0.5 M Na_2SO_4 aqueous electrolytes. It is a promising candidate in the field of energy storage applications.

2. EXPERIMENTAL SECTION

2.1 Materials

The AC and MWCNTs were synthesized in the laboratory. N-Methyl pyrrolidone (NMP 99.95 %), super carbon black (SP) and Polyvinylidene fluoride (PVDF) were purchased from Sigma-Aldrich. Sodium sulfate (Na_2SO_4) and sulphuric acid (H_2SO_4) used to prepare the electrolytes were of analytical grade.

2.2 Synthesis of Activated Carbon

The AC samples were prepared by chemical activation using the shells of *Pongammia pinnata*, collected from Erode region, India. The dried shell was thoroughly washed, dried in an oven at 90 ºC for 24 hours and then crushed into a fine powder. The fine powder was carbonized using a muffle furnace at 450 ºC for 1 hour at a heating rate of 5 ºC min^{-1}. Then, KOH was added to this in a 1:3 mass ratio. The mass was taken in the quartz boat, placed in a quartz tube, and heated in a tubular furnace at 800 ºC for 1 hour for activation under an N_2 atmosphere. The resulting nanoporous activated carbon was stirred with 1M HCl for 1 hour, and washed with double distilled water until neutralization was achieved. Finally, the sample was dehydrated at 80 ºC for 12 hours and ground well into fine powder. The entire preparation process is schematically represented in Fig. 1.

2.3 Preparation of Multi-walled Carbon Nanotubes

The MWCNTs were prepared from *Pongammia pinnata* oil precursor by Spray pyrolysis. The Fe/Co/Mo supported with silica catalyst was mixed thoroughly with methanol suspension of silica (Merck). After evaporating the solvent, the solid was heated at 90-100 °C for 3 hours, ground well and subjected to calcination for 1 hour at 450 °C. After that, it was powdered again and loaded into the reactor. The quartz tube was deoxygenated using N_2 gas at 100 mL/min. Gradually, the temperature was increased to 650 ºC. After spray pyrolyzing for 45 min, the furnace temperature was brought back to 25 ºC. The final mass of carbon was in the form of MWCNTs. It was purified as follows. Then an acidic slurry was prepared by adding 20 ml 1 N HCl to 40 mg of the raw MWCNTs, heating up to 60 ºC and stirring at 600 rpm. The acidic slurry (20 ml) was added to H_2O_2 to form an oxidative slurry, which was then heated and stirred for about 30 minutes. The above addition process was repeated more than two times. The addition of 1 N HCl did the phase separation process. The collected sample was dried at 120 ºC in a hot air oven for 2 hours. The entire process is schematically represented in Fig. 2.

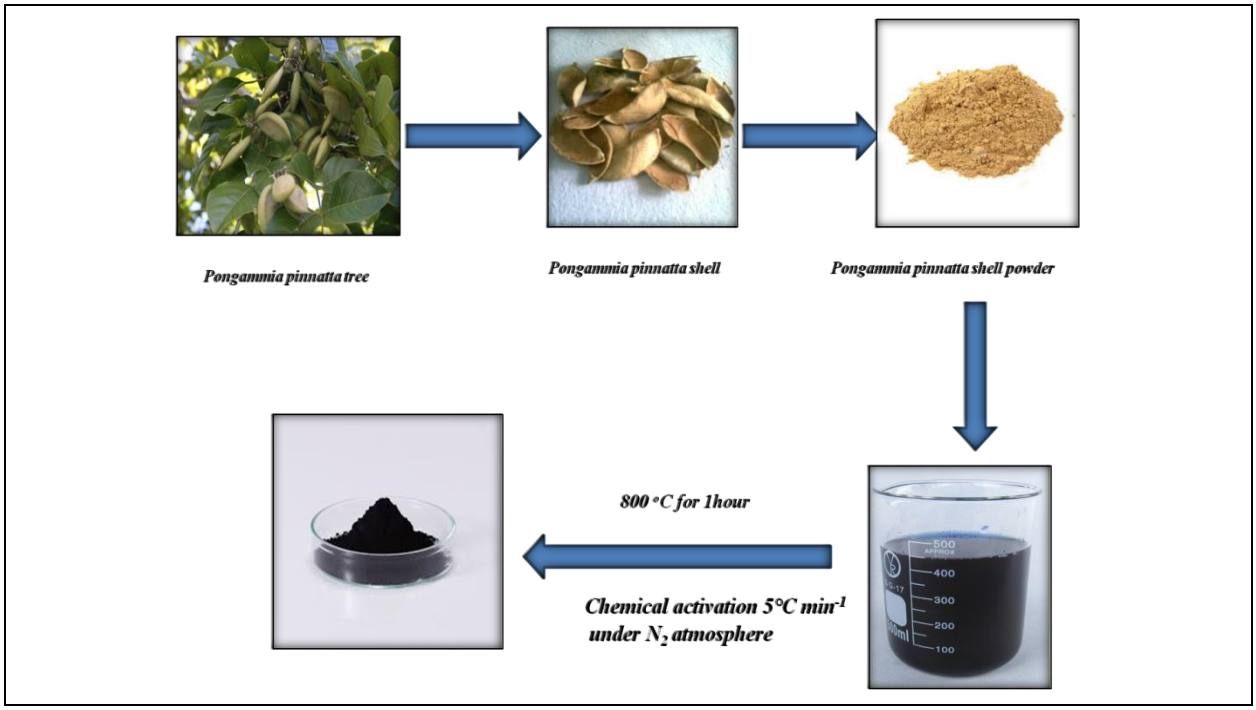

Fig. 1: Schematic representation of preparation of Activated carbon from *Pongammia pinnatta* shell.

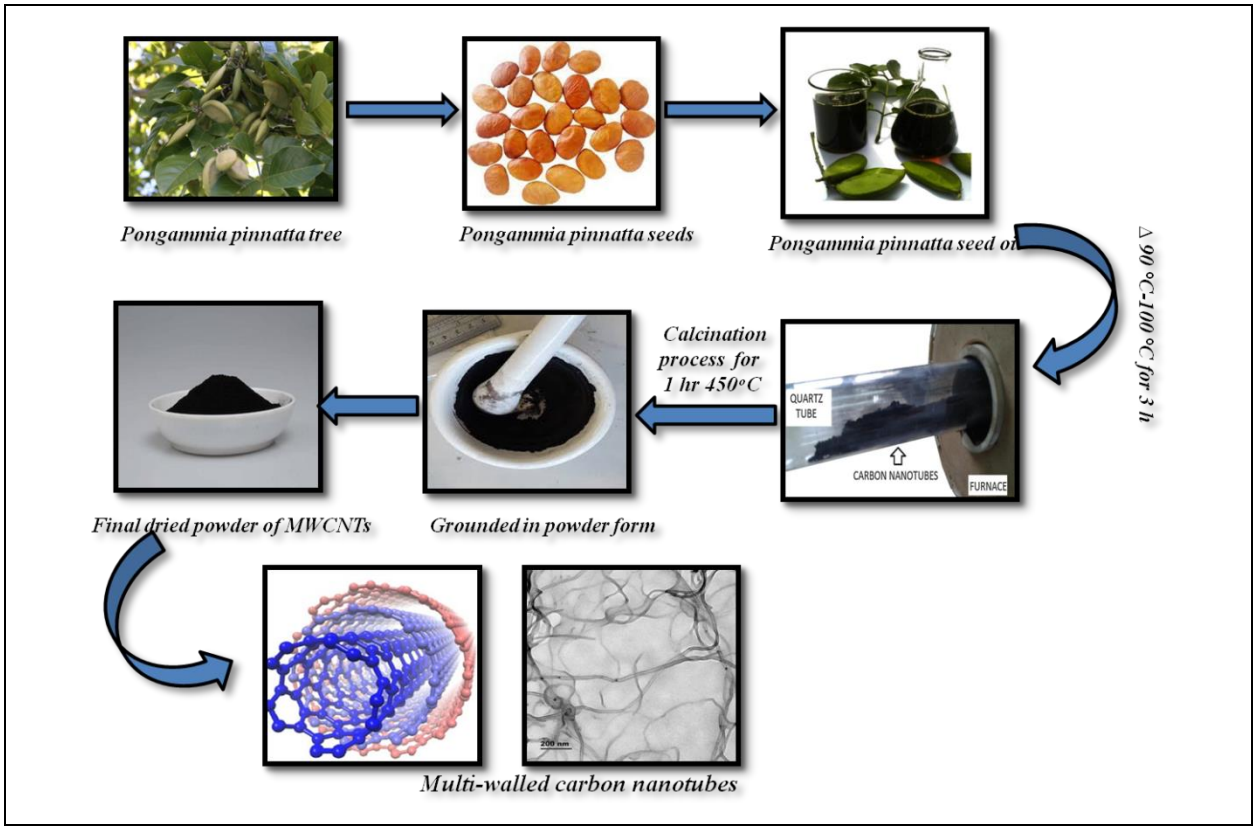

Fig. 2: Schematic representation of preparation of Multi-walled carbon nanotubes from *Pongammia pinnatta* oil.

2.4 Preparation of Stainless Steel (SS) and Graphite Current Collector Electrode

Stainless steel (316 L grade) electrode of 30 µm thickness was used as the current collector. This electrode is flexible. The elemental composition of stainless steel was C-0.03%, Mn-2%, Si-0.750%, P-0.045%, S-0.03%, Cr-16.5%, Mo-2% and Ni-10%, as specified by the manufacturers. The SS foil was etched using an emery paper without the formation of wrinkles and pretreated by soaking it in 5% NaOH for 3 min, followed by rinsing with tap water. It was allowed to dry and soaked in 1% HCl for 30 seconds. After drying the sample, it was washed with deionized water to remove any impurities. Finally, it was rinsed with acetone and then allowed to dry.

Graphite electrode (GE), 250 µm thick, was used as a flexible current collector. The Graphite electrode is slightly etched and pretreated to obtain a fine and uniform coating.

2.5 Preparation of AC-MWCNTs (25:75) SS and AC-MWCNTs (25:75) GE

The electrode material was prepared using the synthesized AC, MWCNTs and SP with the composition (80:10:10) ratio. Activated carbon (80 wt. %), carbon nanotubes (2.5 wt. %), super carbon black (7.5 wt. %), PVDF binder (10 wt.%) and PVP (0.005wt.%) were dispersed in NMP by stirring the mixture using a magnetic stirrer with a hot plate for 8-12 hours. The viscous slurry was applied to the pretreated (Jeżowski, *et al.* 2015) (1×1 cm^2) SS foils and Graphite paper, respectively, using a film applicator. Then, the coated film was allowed to dry overnight at 80 ºC until NMP completely evaporated to enhance the good adhesion of coated materials at 120 ºC for 12 hrs. The prepared electrode materials were dried in a hot air oven and cooled at room temperature. The as-obtained AC-MWCNTs (25:75) SS electrode and AC-MWCNTs (25:75) GE were subjected to an electrochemical test in the three-electrode system using 0.5 M Na_2SO_4 aqueous electrolyte.

2.6 Characterization of the Electroactive Materials

The specific surface area, average pore size and micropore and macropore volumes of AC were measured by N_2 adsorption–desorption isotherm at 77 K using a micro metrics Belsorp surface analyzer. In this measurement, the precursor materials were degassed at 300 ºC under vacuum (10^{-3} m bar) for 5 hours. Brunner-Emmett-Teller (BET) method was employed to determine the specific surface area (SSA). Pore size distribution of AC and MWCNT samples was analyzed using the Barrett-Joyner-Halenda model (BJH). Total pore volume and diameter were analyzed using the NLDFT/GCMC pore size distribution analyzer (P/P_0 of 0.96). The total pore volume and pore diameter of MWCNT were determined using MP-PLOT. The surface morphology of the AC and MWCNT materials was studied using a Scanning electron microscope (BRUKER analytical ultra-high-resolution SEM, Japan) and EDAX was used to examine the elemental compositions of the samples. The crystalline nature and SAED pattern of AC and MWCNT materials were analyzed by X-ray diffraction (XRD, Spinner stage with 8185), XPS X-Ray 024 400µm - FG ON (400 µm) carried at point analysis, Raman spectroscopic analysis and High-resolution transmission electron microscope (HR-TEM (JEOL JEM2100) operating voltage 200 kV).

2.7 Electrochemical Measurement

The electrochemical properties of AC-MWCNTs (25:75) SS electrode and AC-MWCNTs (25:75) GE were investigated using a three-electrode system (SP-150 Biologic electrochemical workstation). The electrode under study was made as the working electrode, while a silver/silver chloride electrode and a platinum wire acted as the reference and counter electrodes, respectively. The coated steel sheet weight was calculated before and after coating to obtain the mass of active material (2-3 mg). The performance of AC-MWCNTs (25:75) SS electrode and AC-MWCNTs (25:75) GE was analyzed by cyclic voltammetry (CV), Galvanostsic charge-discharge measurement (GCD) and electrochemical impedance spectroscopy (EIS), using 0.5 M Na_2SO_4 electrolyte (Barzegar *et al.* 2015). In the CV experiments, the negative potential window was from (-1 V up to 0 V) with various scan rates ranging from 5 to 100 mVs^{-1}. The GCD measurements of SS electrode and GE were carried out at different current densities from (1 to 15 mAg^{-1}) and (2 to 20 mAg^{-1}), respectively. The EIS measurements were recorded in the frequency range of 0.01 -100 kHz, with AC amplitude of 10 mVs^{-1}. All these electrochemical measurements were performed on a SP-150 Biologic electrochemical workstation.

The specific capacitance (C_{sp} in Fg^{-1}) was calculated following a reported (Maher *et al.* 2021; Sivachidambaram *et al.* 2017) equation (1) using the data obtained for AC-MWCNTs electrode from GCD and CV measurements.

$$C_{sp}=I/m*\Delta t / \Delta v \quad \text{----------} \quad (1)$$

Where, I (A) is the current during discharge, m (g) is the mass of active material, Δt (s) is the time during discharge, Δv (V) is the voltage window. The specific energy (SE, $Whkg^{-1}$) and specific power (SP, Wkg^{-1}) were calculated according to Eqs (2) and (3).

The columbic efficiency (η%) was calculated from GCD measurements using equation (4)

$$SE = C_{sp} (\Delta v)^2 \times 1000 / 7200 \text{ ---------- (2)}$$

$$SP = SE / t_{Discharge} \times 3600 \text{ ---------- (3)}$$

$$(\eta\ \%) = t_d / t_c \times 100 \text{ ---------- (4)}$$

where, t_d and t_c are discharge and charging times, respectively.

3. RESULTS AND DISCUSSION

3.1 XRD, XPS and Raman Spectroscopic Analysis of Activated Carbon and MWCNTs

The crystalline structures of the AC and MWCNTs were analyzed by X-ray diffraction. Fig. 3(a) shows the highest two diffraction peaks of the AC in the 2θ range - 24.2° and 43.86°. The diffraction peaks attributed to (002) and (100) graphitic planes confirmed the presence of in-plane conductivity. It signifies a high degree of disorder, which is very common in carbonaceous materials. These resulting XRD patterns are in good accordance with standard ICDD data (98-005-2230) that resemble with ICDD98-018-2760 and 98-017-2292 (Abdessalem Omri and Mourad Benzina, 2012; Gomes Ferreira de Paula *et al.* 2019). The analysis confirmed the structure of the activated graphitic carbon as hexagonal and monoclinic. Similarly, Fig. 3(b) shows the diffraction peak of MWCNTs. A sharp peak at 25.75°and a small peak in the range of 42.9°revealed that the MWCNTs have a regular and orderly arrangement of carbon atoms with a higher degree of crystallinity and conductivity (Saravanan *et al.* 2014; Soleimani *et al.* 2015; Angulakshmi *et al.* 2012). The diffraction peaks showed (002), (100) plane for CNT between the 2θ range of 25.75° and 42.9°. These peaks were indexed according to standard ICDD card data (98-061-7290) and resemble ICDD 98-016-0323. The Raman spectrum of activated carbon, shown in Fig. 3(c), displayed a peak at 1327 cm^{-1} for defective graphite-like material (D band) due to the presence of carbon material at the edge plane and another characteristic G band at 1587 cm^{-1} due to the C-C stretching vibrations of graphitic materials, which is typical for all the sp^2 carbon materials (Ahmed *et al.* 2018). The carbon samples resulted in Id/Ig ratios in the range of 1.10 to 1.42, representing the formation of amorphous graphitic carbon with negligible defects. Likewise, the Raman spectrum of MWCNTs. Fig. 3(d) exhibited two distinct peaks at 1586 cm^{-1} (G band) and 1328 cm^{-1} (D band). The D band arises due to defects and other carbonaceous impurities; the G band occurs due to stretching the C-C bond specifying the graphitic nature and good structural integrity. The above analysis's relative intensity ratio *Id/Ig* has indicated the sp^2/sp^3 bonding ratio parameters. The sp^2 cluster size and reciprocal of the crystalline size along a basal plane (1/La) were measured from X-ray diffraction (Tuinstra and Koenig, 1970; Cuesta *et al.* 1994; Shimodaira *et al.* 2002; Munir *et al.* 2015). XPS spectral analysis of activated carbon confirms that three distinct peaks at 285.98, 531.96 and 398.57 eV were due to carbon, oxygen and nitrogen, respectively. Fig. 4(a) depicted XPS high-resolution spectrum and Fig. 4(b) C1s scan showed a major peaks at 284.96 eV and 285.98 eV confirming C-C/C-H, O-C-O and -C=O, O-C=O. The binding energy at 398.57 eV has indicated the presence of an amino group, pyridine and pyrrole attached to the aromatic ring in the N1s region. Fig. 4(c) O1s scans has displayed two peaks at 531.80 eV and 531.96 eV corresponding to C-OH/C-O-C groups (Kishore *et al.* 2010; Figueiredo *et al.* 1999; Lennon *et al.* 2002). The EDAX analysis from XPS-spectroscopic analysis of activated carbon is listed in Table 2. The obtained EDAX results are in good agreement with the XPS analysis. The peaks at 42.9° revealed the presence of nickel, gallium and manganese in the multi-walled carbon nanotubes. The EDAX results agree with the XRD analysis (Soleimani *et al.* 2015).

3.2 Surface Morphology

The surface chemistry of activated carbon has been characterized by surface area, external surface area, V_{micro}, S_{micro}, average pore diameter, pore width, total pore volume, t-plot measurement, adsorption isotherm studies, porosity, bulk density, specific gravity, ash content, moisture content, pH measurement and conductivity, TDS Analysis, P_{zc} point zero surface charge by mass titration method, percentage of matter soluble in water, percentage of matter soluble in 0.25 M HCl, percentage of carbon yield and presence of volatile matter in %. The above characteristic studies have been reported in Table 1.

3.2.1. N_2 Adsorption-desorption analysis

Surface analysis of AC was studied by N_2 adsorption-desorption analysis at 77 K. The samples were degassed at 300 ºC for 5 hours before the experiments using an NLDFT/GCMC pore distribution analyzer. The surface area, mesopore volume, total pore volume and pore diameter of the AC sample were 1170 m^2/g, 268.98 cm^3/g, 0.5907 cm^3/g and 2.018 nm, respectively. The samples were obtained through the adsorption branch at $P/P_0 > 0.5$ and the total pore volume was determined by the quantity of nitrogen gas adsorbed with relative pressure (P/P_0) of 0.990 and the specific surface area was estimated to be 1170 m^2/g. Fig. 5(a, b and c), show Type I adsorption isotherm, total surface area and pore size analysis of activated carbon. It describes the adsorption of gas molecules to the adsorbents having a microporous structure and hysteresis loop with high relative pressure corresponding to a mesoporous structure for the AC sample (Liu *et al.* 2017; Xu *et al.* 2020). Similarly, the surface area, mesoporous

volume, total pore volume and pore diameter of MWCNTs were 216.12 m^2/g, 49.654 cm^3/g, 1.5067 cm^3/g and 27.887 nm, respectively. Fig. 5(d, e and f) show Type IV adsorption isotherm, total surface area and pore size distribution analysis of MWCNTs, respectively. The mesoporous value has confirmed Type IV isotherm. The small surface area of MWCNTs contributes to the double-layer capacitor.

Based on the pore size distribution classification, there are three classes of pore sizes: micropores (< 2 nm), mesopores (2 ~ 50 nm) and macropores (> 50 nm) (Conway, 1999; Frackowiak *et al.* 2000). The surface area of most activated carbon electrode materials tends to be microporous (Frackowiak, 2001). Considering this principle, since the size of the pores is greater than 0.5 nm, they are electrochemically accessible for aqueous electrolytes. Mesoporous carbon materials are suitable for electrical double-layer capacitors (Kastening and Spinzig, 1986; Mayer *et al.* 1993; Tanahashi *et al.* 1990; Show, 2012). This relation for surface area and pore size of carbon material has a promise of achieving high specific capacitance.

Table 1. Selected properties of *Pongammia pinnata* shell activated carbon.

S. No.	Properties	Value
1	BET surface area, m^2/gm	1175
2	S_{Ext}, m^2/gm	321.47
3	V_{micro}, cm^3/gm	270.27
4	S_{micro} m^2/gm	854.21
5	V_{tot}, cm^3/gm	0.6154
6	Bulk density, g/cm^3	0.587
7	Ash content, %	5.0
8	Moisture content, %	20.9
9	Porosity, %	83.9
10	Specific gravity, S	0.72
11	Matter soluble in water, %	3.28
12	Matter soluble in 0.25 M HCl acid, %	1.2
13	Iodine number, mg/g	1004.34
14	Ph	9.8
15	Conductivity, mS/cm	0.380
16	TDS	190
17	P_{zc} (point zero surface charge)	8.9
18	Yield, % (purity)	69.1
19	Volatile matter, %	5.0

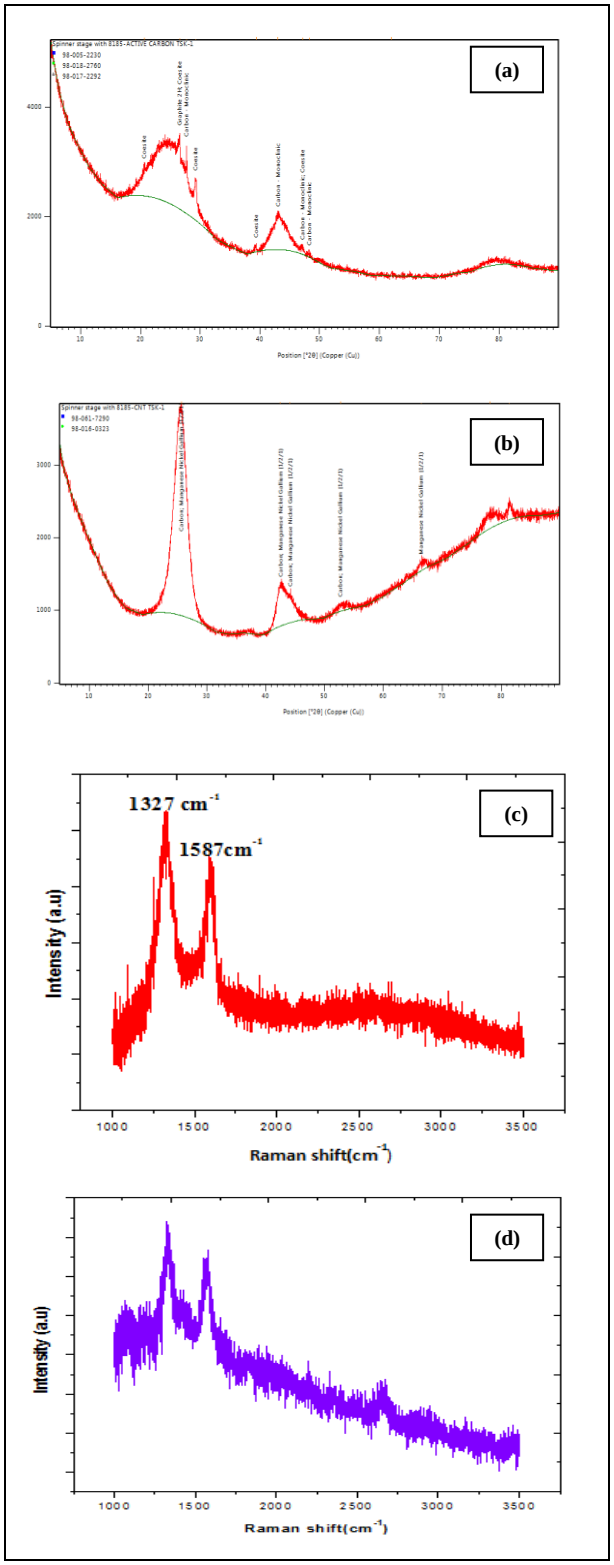

Fig. 3: XRD of (a) activated carbon, (b) multi-walled-carbon nanotubes and Raman spectroscopy of (c) activated carbon and (d) multi-walled-carbon nanotubes.

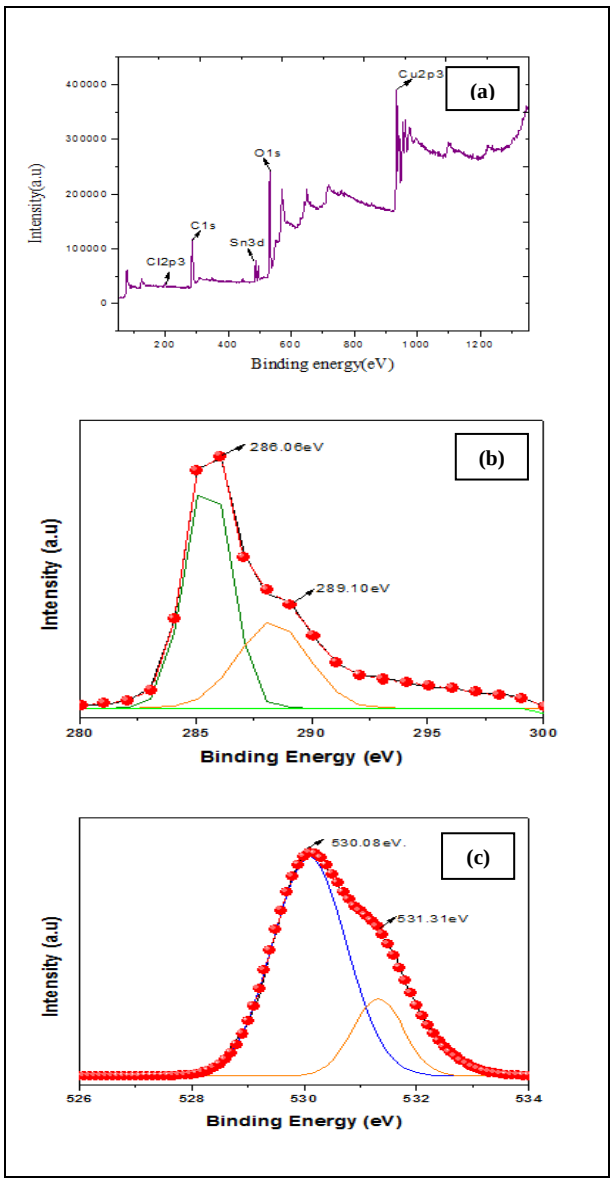

Fig. 4: XPS spectroscopic analysis of (a) Activated carbon, (b) C1s scan and (c) O1s scan.

Table 2. Elemental composition of Activated carbon in XPS analysis.

Name	Peak BE	FWHM eV	Area (P) CPS. eV	Atomic weight [%]	Q
Cu2p3	934.56	4.07	1426394.71	15.50	1
O1s	531.96	3.81	725476.07	33.22	1
Sn3d	487.14	2.82	182604.96	0.62	1
C1s	285.98	3.39	354931.95	39.32	1
Cl2p3	199.38	3.59	33831.78	2.00	1
In3d	445.03	2.61	35316.39	0.14	1
C1s	284.96	1.56	44505.87	4.93	1
N1s	398.57	0.52	3893.44	0.28	1
O1s	531.80	3.14	87343.55	4.00	1

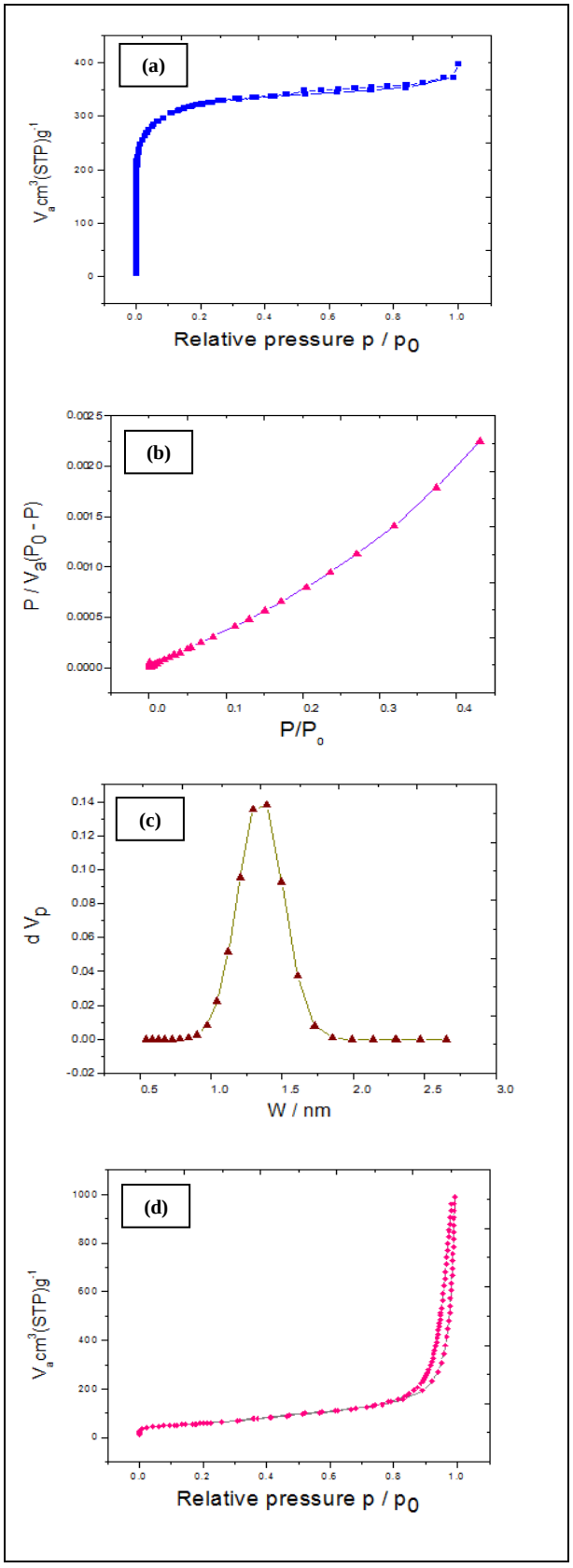

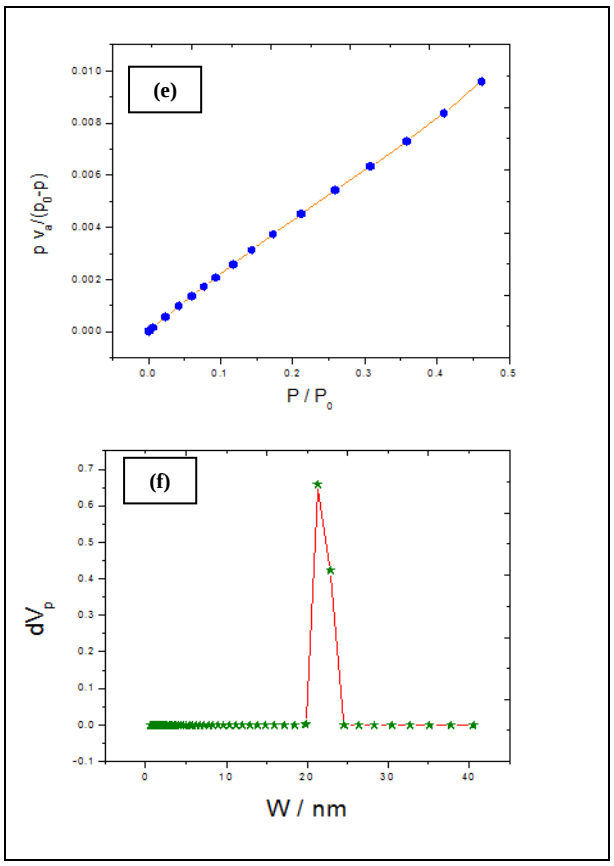

Fig. 5: Morphological characteristics of (a) N_2 adsorption-desorption isotherm for AC, (b) Total surface area vs. pore size for AC, (c) 2D-NLDFT pore size distribution for AC, (d) N_2 adsorption-desorption isotherm for MWCNTs, (e) Total surface area vs pore size for MWCNTs and (f) 2D-NLDFT pore size distribution for MWCNTs.

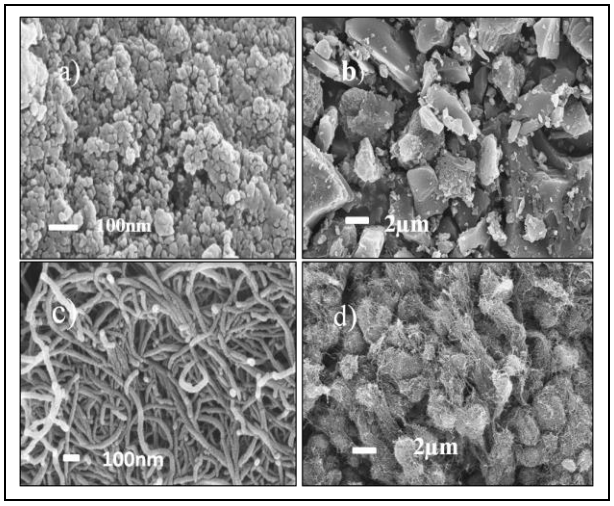

Fig. 6: FESEM images of (a, b) Activated carbon and (c, d) Multi-walled carbon nanotubes.

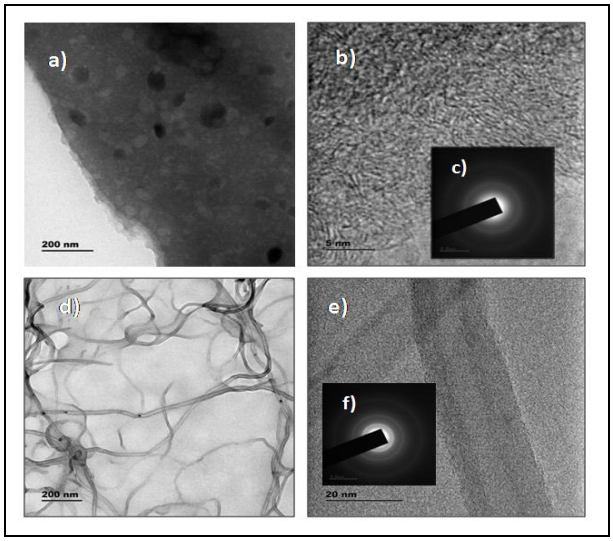

Fig. 7: HR-TEM images of (a, b) Activated carbon, (c) Inset SAED pattern, (d, e) Multi-walled carbon nanotubes (MWCNTs) and (f) Inset SAED pattern.

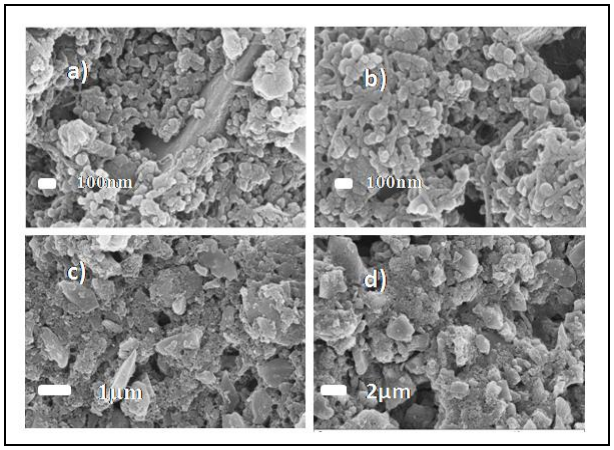

Fig. 8: (i) FESEM & mapping images of (a-d) AC-MWCNTs (25:75) electrode.

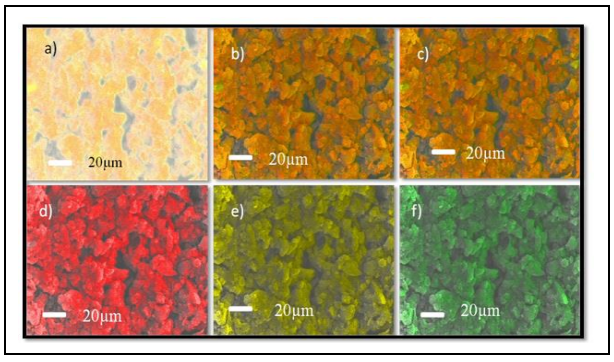

Fig. 8: (ii) FESEM image of (a-f) AC-MWCNTs (25:75) electrode.

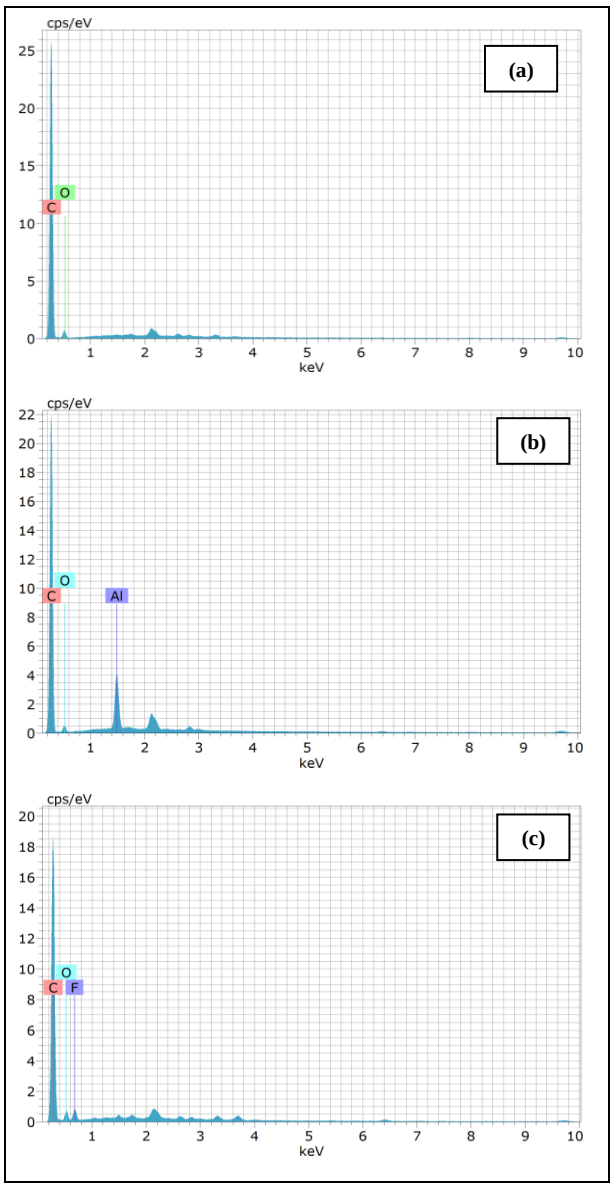

Fig. 9: EDAX analysis of (a) Activated carbon, (b) Multi-walled carbon nanotubes and (c) AC-MWCNTs (25:75) electrode.

3.2.2 Morphological studies

The size and composition of the samples were studied by FESEM and HR-TEM analysis. Fig. 6 (a, b) & (c, d) shows the SEM micrographs of AC and MWCNTs. The surface of activated carbon is planar and porous in nature. It contains large pores of different sizes and shapes. The enhanced surface area was obtained by KOH activation for fine porous structure (Mistar *et al.* 2020; Yoshida, 1993). The high-resolution TEM analysis was proper to identify the electroactive sites that improve the charge storage capacity of the active materials. These results support the quasi-spherical structural behavior and porosity. Fig. 7 (a, b) & (d, e) shows HRTEM images of AC and multi-walled carbon nanotubes. The multi-walled carbon nanotubes were wire-shaped in structure (Palisoc *et al.* 2020). The inset image Fig. 7 (c, f) SAED pattern revealed a hexagonal and monoclinic structure of activated carbon (Inagaki, 2000) and multi-walled carbon nanoparticles, respectively. The electron diffraction (EDP) pattern of MWCNTs showed many rings resembling atomic planes (Asadabad *et al.* 2016). These SAED pattern results reveal that all the layers were having nearly the same chirality, and they confirmed with the XRD results.

In these AC-MWCNTs (25:75), most of the activated carbon has larger particles exposed outside and smaller particles finely coated with MWCNTs (Fig. 8).

3.2.3 EDAX analysis

The elemental compositions of AC and MWCNTs and AC-MWCNTs (25:75) electrodes were studied by EDAX analysis. Fig. 9 (a, b and c) show the EDX spectrum of AC, MWCNTs and AC-MWCNTs (25:75) electrodes, respectively. The AC sample consists of carbon and oxygen and MWCNTs consist of carbon, oxygen, and aluminum. AC-MWCNTs (25:75) electrode contains carbon, oxygen and fluorine. Relevant data were listed in Tables 3, 4 and 5.

Table 3. Elemental composition of Activated carbon.

Element Series	Mass weight [%]	Normal weight [%]	Atomic weight [%]	Error (3 sigma) [wt.%]
Carbon K-series	89.17	89.17	91.64	31.41
Oxygen K-series	10.83	10.83	8.36	6.51
Total:	100.00	100.00	100.00	

Table 4. Elemental composition of Multi-walled Carbon nanotubes.

Element Series	Mass weight [%]	Normal weight [%]	Atomic weight [%]	Error (3 sigma) [wt.%]
Carbon K-series	88.82	88.82	92.67	30.16
Oxygen K-series	6.71	6.71	5.26	3.75
Aluminum K-series	4.47	4.47	2.07	0.73
Total:	100.00	100.00	100.00	

Table 5. Elemental composition of AC-MWCNTs (25:75) electrode.

Element Series	Mass weight [%]	Normal weight [%]	Atomic weight [%]	Error (3 sigma) [wt.%]
Carbon K-series	83.74	83.74	87.97	28.25
Fluorine K-series	6.40	6.40	4.25	3.09
Oxygen K-series	9.86	9.86	7.77	4.85
Total:	100.00	100.00	100.00	

3.2.4 Density functional theory computational methods

All calculations were performed using the Gaussian 09 program package (Frisch *et al.* 2009) with the aid of the Gauss View visualization program. The ground state geometries were fully optimized using the hybrid B3LYP functional methods in combination with the 6-311G (d, p) basis set (Kruse *et al.* 2012). All geometries were optimized to zero negative vibrational frequency to ensure the global minima. The fractional contributions of various fragments to each density of state (DOS) were calculated by Multiwfn (Lu and Chen, 2012). Chemissian was used for data interpretation (Skripnikov, 2016)

The density functional theory calculations were performed using Gaussian 09 computational codes. The super capacitance behavior of CNT-Carbon-Na_2SO_4 systems was created in Gauss view. Then, we employed density functional theory (DFT) to prove the geometrical structures of CNT-Carbon-Na_2SO_4 on their basal planes. As shown in Fig. 10(a) demonstrates the CNT-Carbon-Na_2SO_4 shows a more polarized electron density. In the case of CNT-Carbon-Na_2SO_4, the electron density is distributed throughout the system in uniform ways. This shows that more charge density can be stored on 0.5 M Na_2SO_4 electrolyte system.

Frontier molecular orbital analysis was employed to obtain the band gap of the CNT-Carbon-H_2SO_4 and CNT-Carbon-Na_2SO_4 systems. Results show that the spin-up and spin-down bands are symmetrical, implying that this study's models are non-magnetic (Mousavi-Khoshdel *et al.* 2015; Yang *et al.* 2015). Fig. 10(b) illustrates the electronic FMO levels of the CNT-Carbon-H_2SO_4 and CNT-Carbon-Na_2SO_4 systems, respectively. The calculated band gaps of 0.50 eV was obtained for the Na_2SO_4 electrolyte systems, respectively, which indicate that the Na^+ ions introduced into the carbon, could, increase the electrical conductivity to some extent. This result agrees with the common understanding of the electrical properties of Na_2SO_4.

The DOS of CNT and carbon with Na_2SO_4electrolyte is determined to reveal their electronic properties. The total DOS near the Fermi level exhibits a low population. The total DOS of the CNT-Carbon-Na_2SO_4 system is depicted in Fig. 10 (c) represents a similar shape near the Fermi level for both systems. The DOS around the Fermi level improved considerably by the Na_2SO_4 electrolyte. To explore the influence of electrolyte groups on the electronic DOS and evaluate the contribution of specific atoms to the total DOS, we calculated the partial densities of states (PDOS) and local densities of states (LDOS) of particular atoms of the CNT, carbon, and Na_2SO_4 electrolyte. The states of all atoms around the Fermi level primarily originate from CNT, carbon and electrolytes, indicating that both CNT and carbon on HOMO and LUMO levels are equally populated, whereas the electrolyte are populated more on HOMO than at the LUMO level (Mousavi-Khoshdel and Targholi, 2015; Song *et al.* 2018).

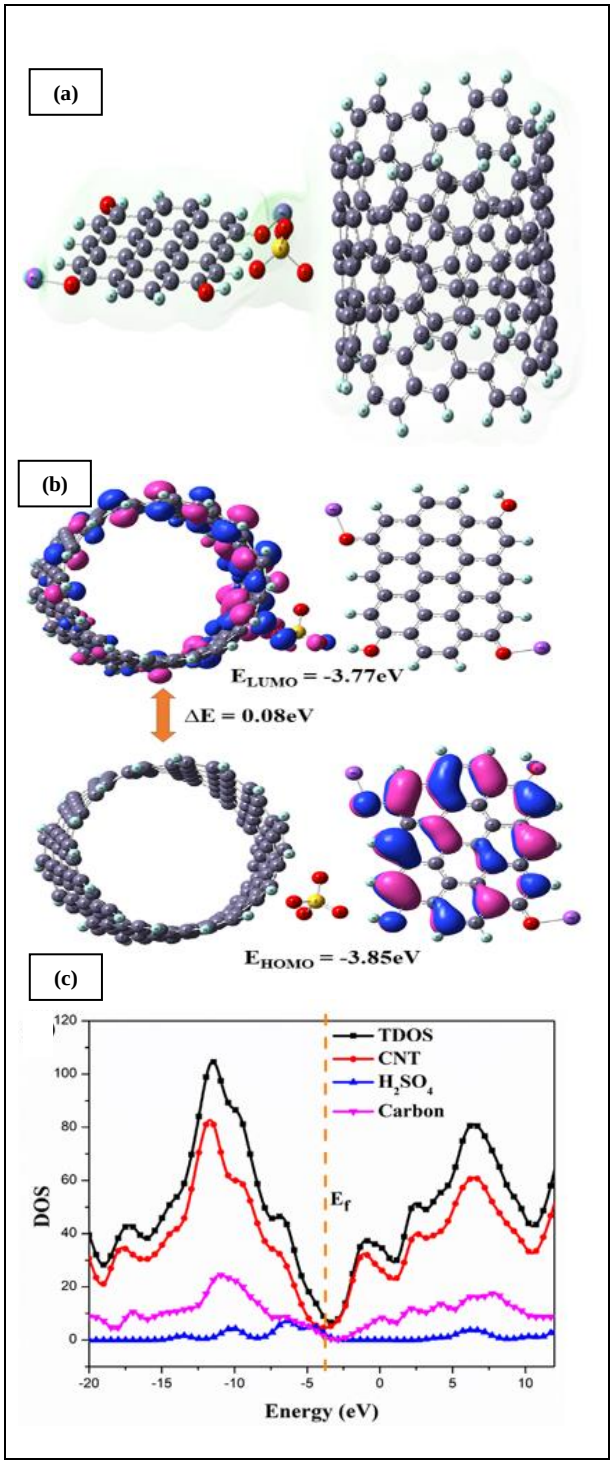

Fig. 10: CNT-Carbon-Na_2SO_4 system of (a) optimized molecular geometry, (b) frontier molecular orbitals and (c) density-of-states plots by DFT/B3LYP method.

3.2.5 Electrochemical measurement of AC-MWCNTs (25:75) SS electrode (Three-electrode system)

Cyclic voltammograms were recorded to assess the performance of AC-MWCNTs (25:75) SS electrode using 0.5 M Na_2SO_4 aqueous electrolytes in a three-electrode system at room temperature at various scan rates (5 to 100 mV s^{-1})and current densities (1 to 15 A g^{-1}) in the negative potential window from (-1 to 0 V). The CV and GCD profile of AC-MWCNTs (25:75) SS electrode shows the high specific capacitance values of 173 Fg^{-1} at the scan rate of 5 mVs^{-1}. Fig. 11a shows the cyclic voltammetric studies of AC-MWCNTs (25:75) SS electrode in 0.5 M Na_2SO_4 electrolyte with various scan rates from 5 to 100 mV s^{-1} in the potential window from -1.0 up to 0 V. It revealed the EDLC behavior of the AC-MWCNTs (25:75) single electrode. The rectangular shape was due to active carbonaceous materials in the electrode and it has a storage mechanism attributed to charge separate states in electrochemical double layer formation. The GCD measurements of AC-MWCNTs (25:75) SS electrode were carried out in the potential window of -1.0 to 0 V against Ag/AgCl at different current densities (1 to 15 mAg^{-1}). Fig. 11b shows the linear charge-discharge curves. It showed the highest specific capacitance of 174 Fg^{-1} at a current density of 1 Ag^{-1}. When the current density has raised from 1 to 15 mAg^{-1}, the specific capacitance and energy density gradually declined from 174 to 0.3 Fg^{-1} and 23.8 $Whkg^{-1}$ to 0.041 $Whkg^{-1}$ in 0.5 M Na_2SO_4 electrolyte. Specific power density has increased from 282.78 to 5000 W kg^{-1} with respect to current densities from 1 to 15 Ag^{-1}. In this, work, the addition of Multi-walled carbon nanotubes in the ratio of (25:75) with respect to 80% of activated carbon exhibits the highest specific capacitance. It is suggested that there is high dependence of the specific capacitance with the applied current. We have optimized the electrode materials' ratios in various combinations of (MWCNTs and SP) with activated carbon such as (25:75) %, (50:50) %, and (75:25) %, respectively. The best outcome results were realized with AC-MWCNTs (25:75) in electrochemical performance. The capacitance strongly decreases when the current density increases. In general, the specific capacitance decreased when the loading percentage of CNTs was too high (Portet *et al*. 2005). The surface morphology of activated carbon and aqueous electrolytes are the positive parameter to enhance the capacitance values (Bichat *et al.* 2010). Fig. 11(c) depicted the impedance spectra in the frequency range of 0.100 to 100 kHz with 10 mVs^{-1}. Electrochemical impedance analysis examines the internal resistance and capacitance of the AC-MWCNTs (25:75) SS supercapacitor electrode (KötzHahn and Gallay, 2006). The electrolyte's effect with constant temperature was investigated. Semicircles were obtained due to porous electroactive materials and electrode-electrolyte interface resistance. From the diameter of the semicircle, it was found to be 3.71 Ω at 67389.8 Hz and R_2 was found to be 4.41 Ω at 82.18 Hz. The obtained specific capacitance and specific energy and power density values of AC-MWCNTs (25:75) SS using 0.5 Na_2SO_4 electrolytes were listed in Table 6. Fig. 12 (a) shows CV performance of AC-MWCNTs (25:75) SS single electrode at scan rates of 5 mVs^{-1} and GCD performance can be observed at a current density of 2 mA g^{-1} (Fig. 12(b)).

3.2.6. Electrochemical measurement of AC-MWCNTs (25:75) GE (Three-electrode system)

The electrochemical performance of AC-MWCNTs (25:75) GE using 0.5 M Na_2SO_4 aqueous electrolytes in a three-electrode system at room temperature at various scan rates (5 to 100 mVs^{-1}) and current densities (2 to 25 mAg^{-1}) in the negative potential window from (-1 to 0 V) was studied. The CV and GCD profile of AC-MWCNTs (25:75) GE in 0.5 M Na_2SO_4 electrolyte is depicted in Fig. 13 (a, b). The obtained specific capacitance value is 95 Fg^{-1} at the scan rate of 5 mVs^{-1}. Fig. 13 (a) shows the cyclic voltammetric studies of AC-MWCNTs (25:75) GE in 0.5M Na_2SO_4 electrolyte with various scan rates from 5 to 100 mVs^{-1} in the potential window from -1.0 up to 0 V. It shows EDLC behavior of the AC-MWCNTs (25:75) GE single electrode. The rectangular shape was due to porous, surface accessible carbonaceous active materials in the electrode and it has a storage mechanism attributed to charge separate states in electrochemical double layer formation. The GCD measurements of AC-MWCNTs (25:75) GE electrode was carried out in the potential window of -1.0 to 0 V against Ag/AgCl at different current densities (2 to 20 mAg^{-1}). Fig. 13 (b) shows the quasi-triangular shaped charge-discharge curves. It showed the highest specific capacitance of 95 Fg^{-1} at a current density of 2 mAg^{-1}. When the current density climbed from 2 to 20 mAg^{-1}, the specific capacitance gradually declines from 95 to 7.5 Fg^{-1}, and specific energy density decreases from 13.21 to 1.043 $Whkg^{-1}$, respectively. At the same time, specific power density increases from 294.742 to 4957.36 Wkg^{-1} with respect to current densities from 2 to 20 mAg^{-1}. Fig. 13 (c) depicted the impedance spectra in the frequency range of 0.100 to 100 kHz with 10 mVs^{-1} amplitude. Electrochemical impedance analysis can find the internal resistance and capacitance of the AC-MWCNTs (25:75) GE supercapacitor electrode. It revealed the effect of the electrolyte with respect to the constant temperature and voltage investigated. A small semicircle is obtained due to porous electroactive materials and electrode-electrolyte interface resistance. From the EIS Nyquist plot, the diameter of the semicircle R1 was found to be 3.71 Ω at 67389.8 Hz and R_2 was found to be 4.41 Ω at 82.18 Hz. The obtained specific capacitance and specific energy and power density values of AC-MWCNTs (25:75) SS using 0.5 Na_2SO_4 electrolyte are listed in Table 7.

In this current work, the addition of Multi-walled carbon nanotubes (MWCNTs) and super carbon black (SP), (25:75) 10% with 80% of activated carbon results in the highest specific capacitance. Fig. 14 (a)

shows CV performance of AC-MWCNTs (25:75) GE at a scan rate of 5 mVs^{-1}. GCD performance can be observed at a current density of 2 mAg^{-1}, as shown in Fig. 14 (b).

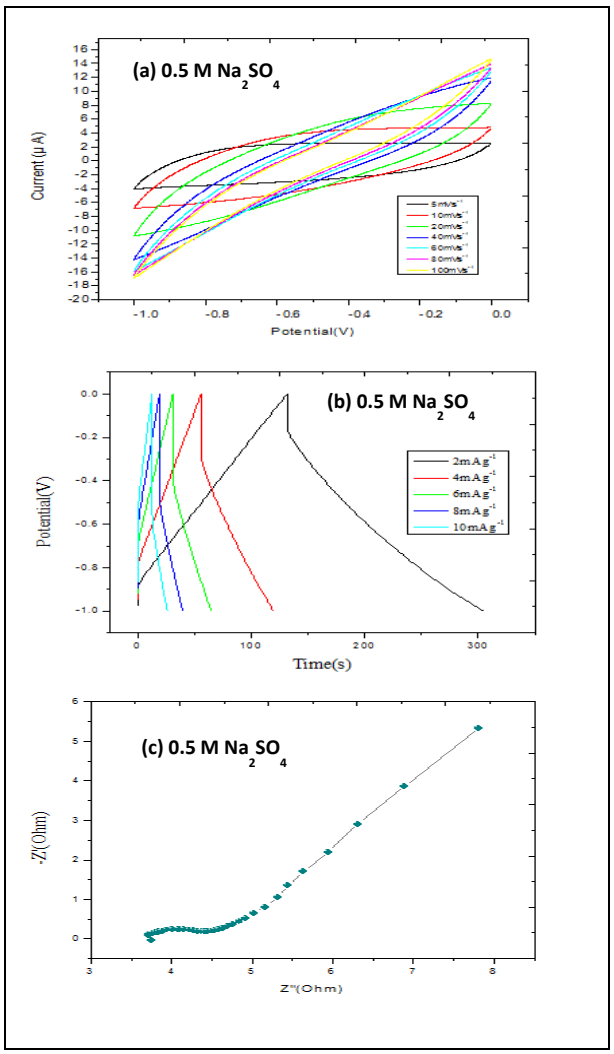

Fig. 11: Electrochemical measurement of AC-MWCNTs (25:75) SS electrode using 0.5 M Na_2SO_4 electrolyte: (a) CV curve at different scan rates, (b) GCD curve at different current densities and (c) Electrochemical impedance spectroscopic studies.

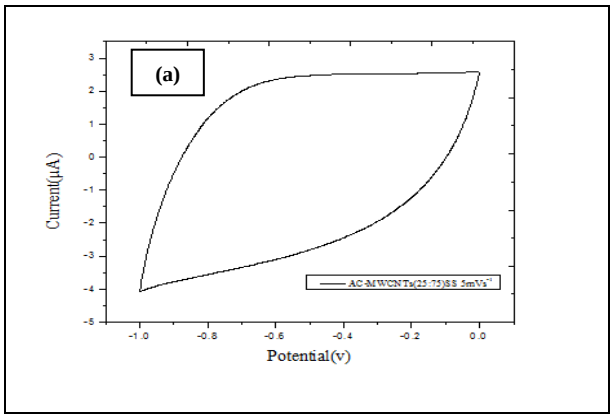

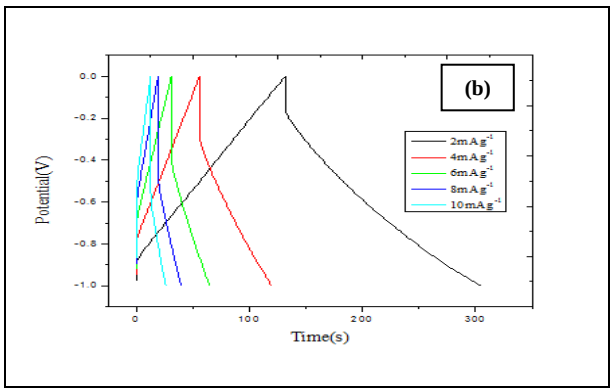

Fig. 12: Electrochemical studies of AC-MWCNTs (25:75) SS electrode using 0.5 M Na_2SO_4 electrolyte: (a) CV curve at 5 mV s^{-1} scan rate and (b) GCD curve at current density of 2 mAg^{-1}.

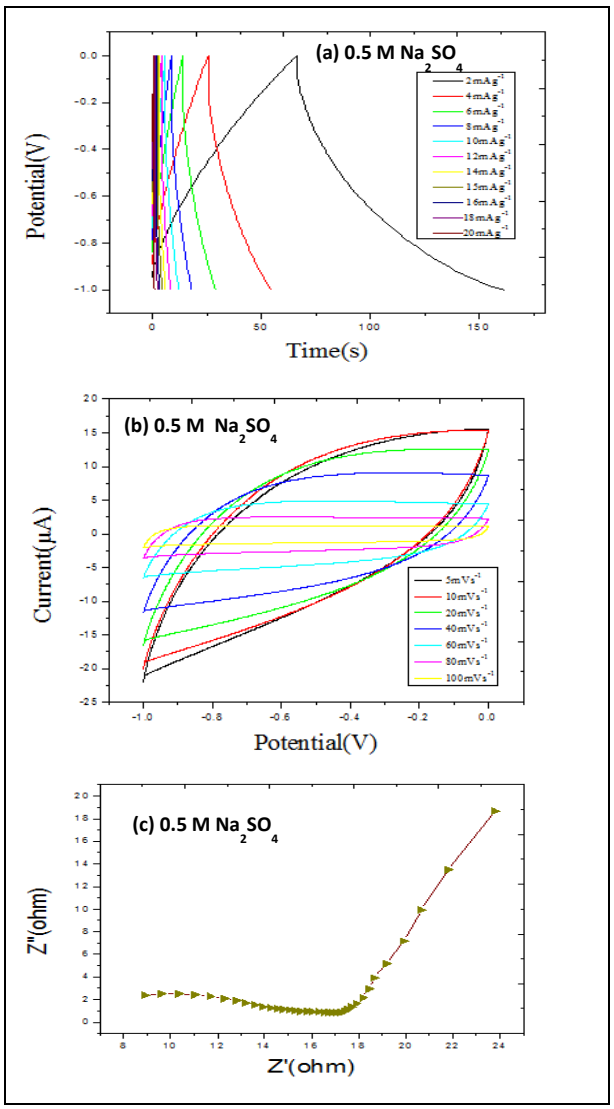

Fig. 13: Electrochemical studies of AC-MWCNTs (25:75) GE electrode using 0.5 M Na_2SO_4 electrolyte (a) CV curve at different scan rates, (b) GCD curve at different current densities and (c) Electrochemical impedance spectroscopic studies.

Table 6. Electrochemical performances of AC-MWCNTs (25:75) SS electrode using 0.5 M Na_2SO_4 electrolyte in a three-electrode system.

Current density (Ag^{-1})	Specific capacitance (Csp, Fg^{-1}) in 0.5M Na_2SO_4	Specific Energy density ($Whkg^{-1}$) in 0.5M Na_2SO_4	Specific Power density (Wkg^{-1}) in 0.5M Na_2SO_4
1	173	23.8	282.78
2	128	17.77	533.1
3	99	13.75	773.43
4	88	12.22	1098
5	75	10.41	1388
6	66	9.16	1736
7	49	6.805	2041.5
8	40	5.55	2497.5
9	18	2.5	2250
10	13	1.805	2707.5
15	0.3	0.041	5000

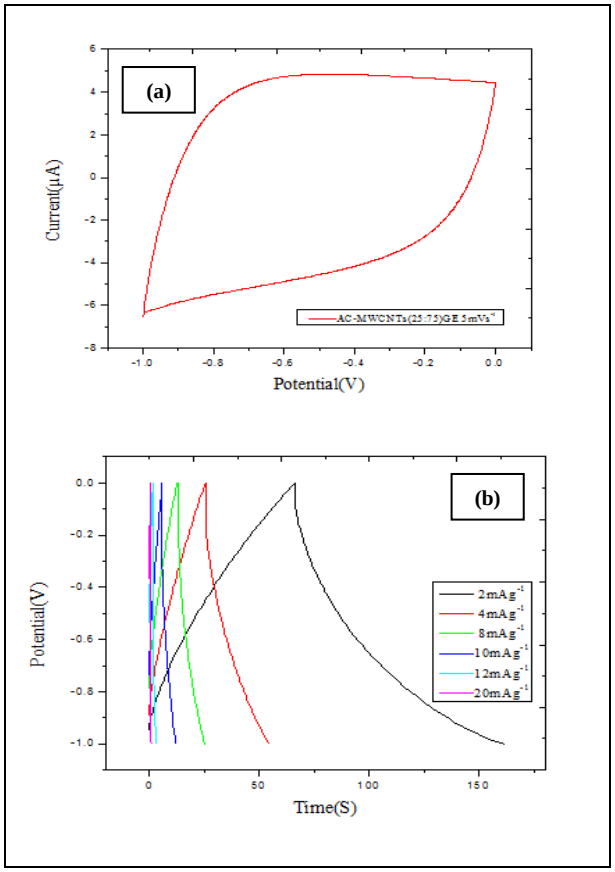

Fig. 14: Electrochemical measurement of AC-MWCNTs (25:75) GE using 0.5 M Na_2SO_4 electrolyte: (a) CV curve at 60 mVs^{-1} scan rate (b) GCD curve at different current densities.

Comparative electrochemical performance of the above two SS and GE electrode were studied. Cyclic voltammetric (CV) performance of AC-MWCNTs (25:75) SS and AC-MWCNTs (25:75) GE single electrodes at scan rates of 5 mVs-1was depicted in Fig. 15 (a). Both electrodes have quasi-rectangular CV curves, which confirms that the characteristics of electrical double layer capacitance (EDLCs) behavior.AC-MWCNTs (25:75) SS resulted in higher specific capacitance than AC-MWCNTs (25:75) GE due to its expanded area of the CV curve. Galvanostatic charge-discharge (GCD) curves at 2 mA g^{-1} is depicted in Fig. 15 (b). The GCD curve of AC-MWCNTs (25:75) SS has exhibited incredible triangle and it revealed the suitable double-layer capacitance.

Fig. 11 (c) and Fig. 13 (c) have shown the impedance analysis of AC-MWCNTs (25:75) SS and AC-MWCNTs (25:75) GE single electrodes. Based on the impedance curve, the internal resistance of AC-MWCNTs (25:75) SS was smaller than that of AC-MWCNTs (25:75) GE. In addition, the radius of the semicircle for AC-MWCNTs (25:75) SS was smaller, indicating a lower charge transfer resistance. In addition, the slope of AC-MWCNTs (25:75) SS was slightly higher than that of AC-MWCNTs (25:75) GE electrode. (Gao *et al.* 2020). The higher the slope influences, the lower the resistance is when the electroactive materials diffused and transferred into the electrolyte. The above comparative electrochemical performances indicate that the AC-MWCNTs (25:75) SS is more promising for energy storage devices than the AC-MWCNTs (25:75) GE. Comparison with other work was done and shown in Table 8. Many literature surveys revealed the highest supercapacitor performance with significant energy and power densities. Our present work, author is focused on optimizing the various compositions of Multi-walled Carbon nanotubes with activated carbon to enhance the electrochemical performance of the supercapacitor.AC-MWCNTs (25:75) SS high performance supercapacitor electrode is a promising electrochemical systems for future energy and power storage devices.

Table 7. Specific capacitance values of AC-MWCNTs (25:75) GE in 0.5 Na_2SO_4 electrolyte.

Current density (mAg^{-1})	Specific capacitance (Csp, Fg^{-1})	Specific Energy density ($Whkg^{-1}$)	Specific Power density (Wkg^{-1})
2	95.268	13.231	294.742
4	81.37	11.301	999.992
6	60	8.33	1038.09
8	55.13	7.65	1545.75
10	48.49	6.735	2038.33
12	42.21	5.862	2556.632
14	35.64	4.95	3058.702
15	29.86	4.147	2570.388
16	24.128	3.351	4048.95
18	19.062	2.675	4579.17
20	7.516	1.043	4957.36

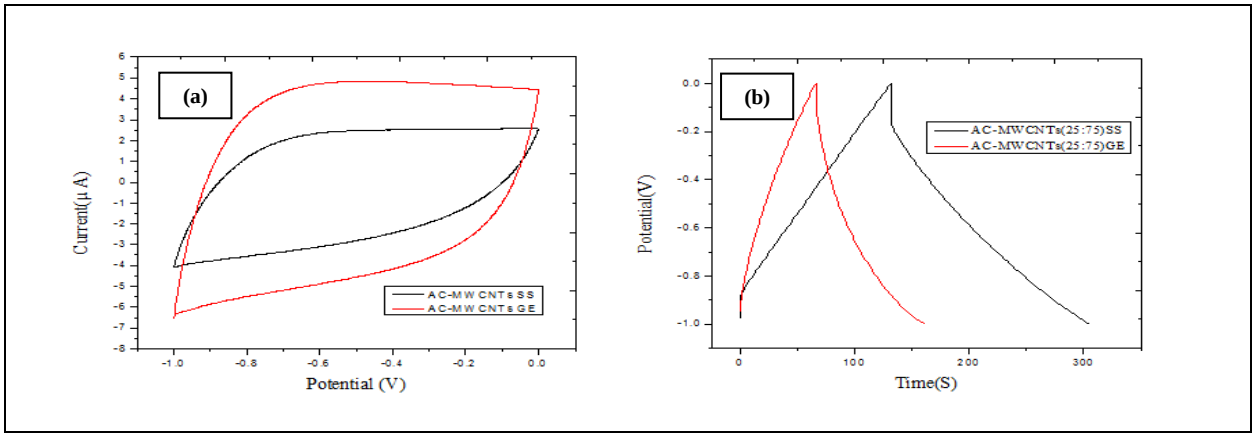

Fig. 15: Comparative electrochemical measurements of AC-MWCNTs (25:75) SS and AC-MWCNTs (25:75) GE electrode using 0.5 M Na_2SO_4 electrolyte: (a) CV curve at 5 mVs^{-1} scan rate and (b) GCD curve at 2 mA g^{-1} current density.

Table 8. Comparison with other literature reports.

Electrode Material	Electrolyte	Specific capacitance (Fg^{-1})	Energy density ($Whkg^{-1}$)	Power density (Wkg^{-1})	References
AC/CNT		96-213	-	-	(Ibukun and Jeong, 2018)
Activated MOFS carbon/MWCNT	3M KOH	122	17 17	1.5	(Palisoc *et al*.2020)
AC	1M KOH	238.2	-	-	(Sivachidambaram *et al*. 2017)
AC	1M H_2SO_4	121 F g^{-1} at 1 A g^{-1} in three-electrode system and 106 F g^{-1} in a symmetric device		361.8 W kg^{-1} with cyclic stability of 100% over 1000 cycles	(Mehare *et al.* 2021)
AC/CNTs	-	93	-	Supercapacitor performances remain stable over 10,000 cycles.	(Portet *et al.* 2005)
N-doped activated carbon (NAC)	6M KOH	168	23.3	2334.3	(Ahmed *et al.* 2018)
AC-SPN-3	6 M KOH 1 M $TEABF_4$ in EC-DEC (1:1)	29.3 μF cm^{-2} 20.1 μF cm^{-2}	10 39	52 286	(Xu *et al.* 2015)
AC	1M 1LiTFSI dispersed in ionic liquid EMITFSI	108.1cycles	51.9	20 kW kg^{-1}	(Ahmed *et al.* 2018)
AC	6 M KOH 1 MEt4NBF4/PC	301 155	32.0 5.2	1370.9 209.4	(Qu *et al.* 2019)
AC-MWCNTs	0.5M Na_2SO_4	173	23.8	282.7	Present work

4. CONCLUSION

The electrochemical performance of AC-MWCNTs (25:75) SS electrode and AC-MWCNTs (25:75) GE were investigated in 0.5 M Na_2SO_4 aqueous electrolytes in three-electrode systems. AC-MWCNTs (25:75) SS electrode in 0.5 M Na_2SO_4 showed an excellent specific capacitance of 173 Fg^{-1} at a current density of 1 mA g^{-1}. The GCD Galvanostatic charge-discharge studies at different current densities in 0.5 M Na_2SO_4, revealed a significant energy density and power density of 23.88 $Whkg^{-1}$ and 282.78 Wkg^{-1}, respectively. Prompted by the results obtained, incorporating electrical conducting materials such as MWCNTs to the activated carbon improved the performance of supercapacitor electrodes in energy storage devices. It seems to be a superior strategy

to meet the requirement of the next generation. AC-MWCNTs (25:75) SS electrode shows superior performance due to the addition of MWCNTs. Further, it enhances the physical properties of activated carbon. Carbon nanotubes are suitable materials for the large-scale production of EDLCs. Our current investigation focused on reaching the domestic and commercial energy requirements in all aspects.

DECLARATION OF COMPETING INTEREST

The authors declare that they have no known competing financial interests or personal relationships that could have appeared to influence the work reported in this paper.

ACKNOWLEDGEMENT

The authors thank Department of Powder Metallurgy ARCI, Hyderabad and Department of Physics, Periyar University, Salem, Tamilnadu, India, for providing facilities for the characterization of samples.

FUNDING

This research received no specific grant from any funding agency in the public, commercial, or not-for-profit sectors.

CONFLICTS OF INTEREST

The authors declare that there is no conflict of interest.

COPYRIGHT

REFERENCE

Simon, P., Gogotsi, Y. and Dunn, B., Where Do Batteries End and Supercapacitors Begin?, *Sci.*, 343(6176), 1210–1211 (2014). https://doi.org/10.1126/science.1249625

Li, C., Islam Md, M., Moore, J., Sleppy, J., Morrison, C., Konstantinov, K., Dou, SX., Renduchintala, C. and Thomas, J., Wearable energy-smart ribbons for synchronous energy harvest and storage, *Nat. Commun.*, 7(1), 1-10 (2016). https://doi.org/10.1038/ncomms13319

Qu, L., Qiao, W., Constant Power Control of DFIG Wind Turbines with Supercapacitor Energy Storage, *IEEE Trans. Ind. Applicat.*, 47(1), 359–367 (2011). https://doi.org/10.1109/TIA.2010.2090932

Aval, L.F., Ghoranneviss, M., Pour, G.B., High-performance supercapacitors based on the carbon nanotubes, graphene and graphite nanoparticles electrodes, *Heliyon.*, 4(11), 1-17 (2018). https://doi.org/10.1016/j.heliyon.2018.e00862

Shi, W., Zhu, J., Sim, D H., Tay, Y Y., Lu, Z., Zhang, X., Sharma, Y., Srinivasan, M., Zhang, H., Hng, H H. and Yan, Q., Achieving high specific charge capacitances in Fe3O4/reduced graphene oxide nanocomposites, *J. Mater. Chem.*, 21(10), 3422-3427 (2011). https://doi.org/10.1039/c0jm03175e

Miller, J.R. and Simon, P., Electrochemical Capacitors for Energy Management, *Sci.*, 321(5889), 651–652 (2008). https://doi.org/10.1126/science.1158736

Brownson, D.A.C., Kampouris, D.K. and Banks, C.E., An overview of graphene in energy production and storage applications, *J. Power Sources.*, 196(11), 4873–4885 (2011). https://doi.org/10.1016/j.jpowsour.2011.02.022

Augustyn, V., Simon, P. and Dunn, B., Pseudocapacitive oxide materials for high-rate electrochemical energy storage, *Energy Environ. Sci.*, 7(5), 1597-1614 (2014). https://doi.org/10.1039/c3ee44164d

Simon, P., Gogotsi, Y., Materials for electrochemical capacitors, *Nat. Mater.*, 7(11), 845–854 (2008). https://doi.org/10.1038/nmat2297

Liu, C., Li, F., Ma, L.P., Cheng, H.M., Advanced Materials for Energy Storage, *Adv. Mater.*, 22(8), E28–E62 (2010). https://doi.org/10.1002/adma.200903328

Ibukun, O. and Jeong, H.K., An Activated Carbon and Carbon Nanotube Composite for a High-Performance Capacitor, *New Phys.: Sae Mulli*, 68(2), 185–188 (2018). https://doi.org/10.3938/NPSM.68.185

Angulakshmi, V.S., Sivakumar, N. and Karthikeyan, S., Response Surface Methodology for Optimizing Process Parameters for Synthesis of Carbon Nanotubes, *J. Environ. Nanotechnol.*, 1(1), 40-45 (2012). https://doi.org/10.13074/jent.2012.10.121019

Mageswari, S., Angulakshmi, V.S., and Sathiskumar, C., Synthesis of Multi-Walled Carbon Nanotubes and Its Application for Removal of Dyes, *Int. J. Adv. Res. Basic Eng. Sci. Technol.*, 3(28), 38-46 (2017).

Karthikeyan, S., Kalaiselvan, S., Manorangitham, D. and Maragathamani, S., Morphology and Structural Studies of Multi-walled Carbon Nanotubes by Spray Pyrolysis using Madhuca Longifolia Oil, *J. Environ. Nanotechnol.*, 2(4), 15–20 (2013). https://doi.org/10.13074/jent.2013.12.132040

Karthikeyan, S., Sivakumar, P. and Palanisamy, P.N., Novel Activated Carbons from Agricultural Wastes and their Characterization, *E-J. Chem.*, 5(2), 409–426 (2008). https://doi.org/10.1155/2008/902073

Sivakumar, B., Kannan, C. and Karthikeyan, S., Preparation and characterization of activated carbon prepared from Balsamodendron caudatum wood waste through various activation processes, *Rasāyan J. Chem.*, 5(3), 321-327 (2012).

Palisoc, S., Dungo, J.M. and Natividad, M., Low-cost supercapacitor based on multi-walled carbon nanotubes and activated carbon derived from Moringa Oleifera fruit shells. Heliyon., 6(1), 1-9 (2020). https://doi.org/10.1016/j.heliyon.2020.e03202

Muthu Balasubramanian, M., Subramani, M., Murugan, D. and Ponnusamy, S., Groundnut shell–derived porous carbon-based supercapacitor with high areal mass loading using carbon cloth as current collector. *Ionics.*, 26(12), 6297–6308 (2020). https://doi.org/10.1007/s11581-020-03754-8

Jain, A. and Tripathi, S.K., Fabrication and characterization of energy storing supercapacitor devices using coconut shell based activated charcoal electrode, *Mat. Sci. Eng.: B.*, 183, 54–60 (2014). https://doi.org/10.1016/j.mseb.2013.12.004

Ahmed, S., Ahmed, A. and Rafat, M., Supercapacitor performance of activated carbon derived from rotten carrot in aqueous, organic and ionic liquid based electrolytes, *J. Saudi Chem. Soc.*, 22(8), 993-1002 (2018). https://doi.org/10.1016/j.jscs.2018.03.002

Zhou, Y., Jin, P., Zhou, Y. and Zhu, Y., High-performance symmetric supercapacitors based on carbon nanotube/graphite nanofiber nanocomposites, *Sci. Rep.*, 8(1), 1-8 (2018). https://doi.org/10.1038/s41598-018-27460-8

Mandal, M., Subudhi, S., Alam, I., Subramanyam, B., Patra, S., Raiguru, J., Das, S. and Mahanandia, P., Facile synthesis of new hybrid electrode material based on activated carbon/multi-walled carbon nanotubes@ZnFe2O4 for supercapacitor applications, *Inorg. Chem. Commun.*, 123, 108332 (2021). https://doi.org/10.1016/j.inoche.2020.108332

Niu, C., Sichel, E.K., Hoch, R. and Moy, D., Tennent, H., High power electrochemical capacitors based on carbon nanotube electrodes, *Appl. Phys. Lett.*, 70(11), 1480–1482(1997). https://doi.org/10.1063/1.118568

Yoon, B.J., Jeong, S.H., Lee, K.H., Seok Kim, H., Gyung Park, C. and Hun Han, J., Electrical properties of electrical double layer capacitors with integrated carbon nanotube electrodes, *Chem. Phys. Lett.*, 388(1–3), 170-174 (2004). https://doi.org/10.1016/j.cplett.2004.02.071

Emmenegger, C.H., Mauron, P.H., Sudan, P., Wenger, P., Hermann, V., Gallay, R. and Züttel, A., Investigation of electrochemical double-layer (ECDL) capacitors electrodes based on carbon nanotubes and activated carbon materials, *J. Power Sources*., 124(1), 321–329 (2003). https://doi.org/10.1016/S0378-7753(03)00590-1

Signorelli, R., Ku, D.C., Kassakian, J.G. and Schindall, J.E., Electrochemical Double-Layer Capacitors Using Carbon Nanotube Electrode Structures, *Proc. IEEE.*, 97(11), 1837–1847 (2009). https://doi.org/10.1109/JPROC.2009.2030240

Hu, L., Choi, J.W., Yang, Y., Jeong, S., La Mantia, F., Cui, L.F. and Cui. Y., Highly conductive paper for energy-storage devices, *Proc. Natl. Acad. Sci. USA.*, 106(51), 21490–21494 (2009). https://doi.org/10.1073/pnas.0908858106

Show, Y., Electric Double-Layer Capacitor Fabricated with Addition of Carbon Nanotube to Polarizable Electrode, J. Nanomater., 2012, 1-8 (2012). https://doi.org/10.1155/2012/929343

Jeżowski, P., Nowicki, M., Grzeszkowiak, M., Czajka, R., Béguin, F., Chemical etching of stainless steel 301 for improving performance of electrochemical capacitors in aqueous electrolyte, *J. Power Sources.*, 279, 555-562 (2015). https://doi.org/10.1016/j.jpowsour.2015.01.027

Barzegar, F., Momodu, D.Y., Fashedemi, O.O., Bello, A., Dangbegnon, J.K., Manyala, N., Investigation of different aqueous electrolytes on the electrochemical performance of activated carbon-based supercapacitors, RSC Adv., 5(130), 107482–107487 (2015). https://doi.org/10.1039/C5RA21962K

Maher, M., Hassan, S., Shoueir, K., Yousif, B. and Abo-Elsoud, M.E.A., Activated carbon electrode with promising specific capacitance based on potassium bromide redox additive electrolyte for supercapacitor application, *J. Mater. Res. Technol.*, 11, 1232–1244 (2021). https://doi.org/10.1016/j.jmrt.2021.01.080

Sivachidambaram, M., Vijaya, J.J., Kennedy, L.J., Jothiramalingam, R., Al-Lohedan, H.A., Munusamy, M.A., Elanthamilan, E. and Merlin, J.P., Preparation and characterization of activated carbon derived from the Borassus flabellifer flower as an electrode material for supercapacitor applications, *New J. Chem.*, 41(10), 3939-3949 (2017). https://doi.org/10.1039/C6NJ03867K

Abdessalem Omri and Mourad Benzina, Characterization of Activated carbon prepared from a new raw lignocellulosic material: ZIZIPHUS SPINA-CHRISTI SEEDS, *J. Soc. Chim. Tunis.*, 14, 175-183 (2012).

Gomes Ferreira de Paula, F., Campello-Gómez, I., Ortega, P.F.R., Rodríguez-Reinoso, F., Martínez-Escandell, M. and Silvestre-Albero, J., Structural Flexibility in Activated Carbon Materials Prepared under Harsh Activation Conditions, *Mat.*, 12(12), 1-12 (2019). https://doi.org/10.3390/ma12121988

Saravanan, A., Prasad, K., Gokulakrishnan, N., Kalaivani, R., Somanathan, T., Efficiency of Transition Metals in Combustion Catalyst for High Yield Helical Multi-Walled Carbon Nanotubes, *adv. Sci. engng. med.*, 6(7), 809–813 (2014). https://doi.org/10.1166/asem.2014.1569

Soleimani, H., Yahya, N., Baig, MK., Khodapanah, L., Sabet, M., Synthesis of Carbon Nanotubes for Oil-water Interfacial Tension Reduction, *Oil Gas Res.*, 1(1), 1-5 (2015). https://doi.org/10.4172/2472-0518.1000104

Angulakshmi, V.S., Sivakumar, N., Karthikeyan, S., Response Surface Methodology for Optimizing Process Parameters for Synthesis of Carbon Nanotubes, *J. Environ. Nanotechnol*., 1(1), 40–45 (2012). https://doi.org/10.13074/jent.2012.10.121019

Ahmed, S., Ahmed, A., Rafat, M., Supercapacitor performance of activated carbon derived from rotten carrot in aqueous, organic and ionic liquid based electrolytes, *J. Saudi Chem. Soc.*, 22(8), 993–1002 (2018). https://doi.org/10.1016/j.jscs.2018.03.002

Tuinstra, F. and Koenig, J.L., Raman Spectrum of Graphite, *J. Chem. Phys.*, 53(3), 1126–1130 (1970). https://doi.org/10.1063/1.1674108

Cuesta, A., Dhamelincourt, P., Laureyns, J., Martínez-Alonso, A., Tascón, J.M.D., Raman microprobe studies on carbon materials, *Carbon*, 32(8), 1523–1532 (1994). https://doi.org/10.1016/0008-6223(94)90148-1

Shimodaira, N. and Masui, A., Raman spectroscopic investigations of activated carbon materials, *J. Appl. Phys.*, 92(2), 902–909 (2002). https://doi.org/10.1063/1.1487434

Munir, K.S., Qian, M., Li, Y., Oldfield, D.T., Kingshott, P., Zhu, D.M. and Wen, C., Quantitative Analyses of MWCNT-Ti Powder Mixtures using Raman Spectroscopy: The Influence of Milling Parameters on Nanostructural Evolution: Quantitative Analyses of MWCNTs-Ti Powder Mixtures, *Adv. Eng. Mater.*, 17(11), 1660–1669 (2015). https://doi.org/10.1002/adem.201500142

Kishore, K.V., Kaza Somasekhara Rao, G., and Vani, K.N.K., X-Ray Photoelectron Spectroscopy Studies on Activated Carbon Prepared From Rind of Citrus nobilis, *Asian J. Chem.*, 22(6), 4377-4381 (2010).

Figueiredo, J.L., Pereira, M.F.R., Freitas, M.M.A. and Órfão, J.J.M., Modification of the surface chemistry of activated carbons, *Carbon*., 37(9), 1379–1389 (1999). https://doi.org/10.1016/S0008-6223(98)00333-9

Lennon, D., Lundie, D.T., Jackson, S.D., Kelly, G.J. and Parker, S.F., Characterization of Activated Carbon Using X-ray Photoelectron Spectroscopy and Inelastic Neutron Scattering Spectroscopy, *Langmuir.*, 18(12), 4667-4673 (2002). https://doi.org/10.1021/la011324j

Liu, Q., Ke, M., Liu, F, Yu, P., Hu, H. and Li, C., High-performance removal of methyl mercaptan by nitrogen-rich coconut shell activated carbon, *RSC Adv*.,7(37), 22892–22899 (2017). https://doi.org/10.1039/C7RA03227G

Xu, L., Zhang, J., Ding, J., Liu, T., Shi, G., Li, X., Dang, W., Cheng, Y. and Guo, R., Pore Structure and Fractal Characteristics of Different Shale Lithofacies in the Dalong Formation in the Western Area of the Lower Yangtze Platform, *Miner*., 10(1), 1-25 (2020). https://doi.org/10.3390/min10010072

Conway, B.E., Electrochemical Supercapacitors || Electrochemical Capacitors Based on Pseudocapacitance, *Springer*, 221–257 (1999). https://doi.org/10.1007/978-1-4757-3058-6_10

Frackowiak, E., Metenier, K., Bertagna, V. and Beguin, F., Supercapacitor electrodes from multi-walled carbon nanotubes, *Appl. Phys. Lett.*, 77(15), 2421–2423 (2000). https://doi.org/10.1063/1.1290146

Frackowiak, E. and Béguin, F., Carbon materials for the electrochemical storage of energy in capacitors, *Carbon*., 39, 937–950 (2001). https://doi.org/10.1016/S0008-6223 (00)00183-4

Kastening, B. and Spinzig, S., Electrochemical polarization of activated carbon and graphite powder suspensions, *J. Electroanal. Chem. Interfacial Electrochem.*, 214(1–2), 295–302 (1986). https://doi.org/10.1016/0022-0728(86)80104-8

Mayer, S.T., Pekala, R.W., Kaschmitter, J. L., The Aerocapacitor: An Electrochemical Double-Layer Energy-Storage Device, *J. Electrochem. Soc.*, 140(2), 446–451 (1993). https://doi.org/10.1149/1.2221066

Tanahashi, I., Yoshida, A. and Nishino, A., Electrochemical Characterization of Activated Carbon-Fiber Cloth Polarizable Electrodes for Electric Double-Layer Capacitors, *J. Electrochem. Soc*., 137(10), 3052-3057 (1990). https://doi.org/10.1149/1.2086158

Show, Y., Electric Double-Layer Capacitor Fabricated with Addition of Carbon Nanotube to Polarizable Electrode, *J. Nanomater.*, 2012, 1–8 (2012). https://doi.org/10.1155/2012/929343

Mistar, E.M., Alfatah, T., Supardan, M.D., Synthesis and characterization of activated carbon from Bambusa vulgaris striata using two-step KOH activation, *J. Mater. Res. Technol.*, 9(3), 6278–6286 (2020). https://doi.org/10.1016/j.jmrt.2020.03.041

Yoshida, H., Fibres: Equilibria Chem, *Eng. sci.*, 48(12), 2267-2272 (1993). https://doi.org/10.1016/0009-2509(93)80242-I

Inagaki, M., Old but New Materials: Carbons In: New Carbons - Control of Structure and Functions; Inagaki, M., Ed., *Elsevier Science: Oxford*, 1–29 (2000).

Asadabad, M.A. and Eskandari, M.J., Electron Diffraction. In: Modern Electron Microscopy in Physical and Life Sciences, *IntechOpen*., (2016). https://doi.org/10.5772/61781

Frisch, M.J., Trucks, G.W., Schlegel, H.B., Scuseria, G.E., Robb, M.A., Cheeseman, J.R. and Scalmani, G., Wallingford CT 201. Gaussian 09, Revision D. 01, *Gaussian Inc*., (2009).

Kruse, H., Goerigk, L. and Grimme, S., Why the Standard B3LYP/6-31G* Model Chemistry Should Not Be Used in DFT Calculations of Molecular Thermochemistry: Understanding and Correcting the Problem, *J. Org. Chem.*, 77(23), 10824–10834 (2012). https://doi.org/10.1021/jo302156p

Lu, T. and Chen, F., Multiwfn: A multifunctional wavefunction analyzer, *J. Comput. Chem.*, 33(5), 580–592 (2012). https://doi.org/10.1002/jcc.22885

Skripnikov, L., Chemissian Version 4.43, Visualization Computer Program, (2016). http://www.chemissian.com

Mousavi-Khoshdel, M., Targholi, E. and Momeni, M.J., First-Principles Calculation of Quantum Capacitance of Codoped Graphenes as Supercapacitor Electrodes, *J. Phys. Chem. C.*, 119(47), 26290–26295 (2015). https://doi.org/10.1021/acs.jpcc.5b07943

Yang, G., Zhang, H., Fan, X. and Zheng, W., Density Functional Theory Calculations for the Quantum Capacitance Performance of Graphene-Based Electrode Material, *J. Phys. Chem. C.*, 119, 6464-6470 (2015). http://dx.doi.org/10.1021/jp512176r

Mousavi-Khoshdel, S.M. and Targholi, E., Exploring the effect of functionalization of graphene on the quantum capacitance by first principle study, *Carbon*., 89, 148-160 (2015). https://doi.org/10.1016/j.carbon.2015.03.013

Song, C., Wang, J., Meng, Z., Hu, F. and Jian, X., Density Functional Theory Calculations of the Quantum Capacitance of Graphene Oxide as a Supercapacitor Electrode, *Chem. Phys. Chem*., 19(13), 1579–1583 (2018). https://doi.org/10.1002/cphc.201800070

Portet, C., Taberna, P.L., Simon, P. and Flahaut, E., Influence of carbon nanotubes addition on carbon–carbon supercapacitor performances in organic electrolyte, *J. Power Sources.*, 139(1–2), 371–378(2005). https://doi.org/10.1016/j.jpowsour.2004.07.015

Bichat, M.P., Raymundo-Piñero, E. and Béguin, F., High voltage supercapacitor built with seaweed carbons in neutral aqueous electrolyte, *Carbon* , 48(15),4351–4361(2010). https://doi.org/10.1016/j.carbon.2010.07.049

Kötz, R., Hahn, M. and Gallay, R., Temperature behavior and impedance fundamentals of supercapacitors, *J. Power Sources.*, 154(2), 550–555 (2006). https://doi.org/10.1016/j.jpowsour.2005.10.048

Mehare, M.D., Deshmukh, A.D. and Dhoble, S J., Bio-waste lemon peel derived carbon based electrode in perspect of supercapacitor, *J. Mater. Sci.: Mater. Electron.*, 32, 14057–14071 (2021). https://doi.org/10.1007/s10854-021-05985-5

Portet, C., Taberna, P.L., Simon, P., Flahaut, E. and Laberty-Robert, C., High power density electrodes for Carbon supercapacitor applications, *Electrochim. Acta.*, 50(20), 4174–4181 (2005). https://doi.org/10.1016/j.electacta.2005.01.038

Ahmed, Sultan., Rafat, M., Ahmed and Ahsan., Nitrogen doped activated carbon derived from orange peel for supercapacitor application, *Adv. Nat. Sci.: Nanosci. Nanotechnol.*, 9(3), 035008 (2018). https://doi.org/10.1088/2043-6254/aad5d4

Xu, J., Gao,Q., Zhang, Y., Tan, Y. and Tian, W., Zhu, L., Jiang, L., Preparing two-dimensional microporous carbon from Pistachio nutshell with high areal capacitance as supercapacitor materials, *Sci. Rep.*, 4, 1-6 (2015). https://doi.org/10.1038/srep05545

hmed, S., Hussain, S., Ahmed, A. and Rafat, M., High performance supercapacitor from activated carbon derived from waste orange skin, *AIP Conf. Proc.*, 1953*(1)*, 1-5 (2018). https://doi.org/10.1063/1.5032522

Qu, X., Liu, Y., Zhang, C., Zhu, A., Wang, T., Tian, Y., Yu, J., Xing, B., Huang, G. and Cao, Y., Effect of diferent pretreatment methods on sesame husk-based activated carbon for supercapacitors with aqueous and organic electrolytes, *J. Mater. Sci.*, 30, 7873–7882 (2019). http://dx.doi.org/10.1007/s10854-019-01107-4

Gao, Yang, Tang, Yakun, Liu, Wei, Liu, Lang, Zeng, Xingya, Porous bamboo-like CNTs prepared by a simple and low cost steam activation for supercapacitors, *Int. J. Energy Res.*, 44(13), 10946-10952 (2020). https://doi.org/10.1002/er.5672